JOURNAL OF MATERIALS SCIENCE **33** (1998) 5247–5254

Use of emanation thermal analysis in characterization of the influence of grinding on textural and structural properties of nanosized titania powders

C. REAL, J. M. CRIADO
Instituto de Ciencia de Materiales de Sevilla, Centro Mixto C.S.I.C., Universidad de Sevilla, c/Americo Vespucio s/n, Isla de La Cartuja, 41092 Sevilla, Spain
E-mail: creal@cica.es

V. BALEK
Institute of Nuclear Research, 25068 REZ, Czech Republic

It is shown that emanation thermal analysis (ETA) is a very sensitive method for studying the textural and structural changes undergone during thermal and/or mechanical treatment of TiO_2. It is shown that the activation energy for the bulk diffusion of radon into titania samples annealed at 1100 °C dramatically increases by increasing the prior grinding time of the sample at room temperature. These results demonstrate that grinding of TiO_2 prior to the annealing treatment considerably improves sintering and densification of the material.

1. Introduction

Anatase and rutile are two of the three polymorphic forms of TiO_2. It has been reported in the literature that anatase → rutile conversion is an exothermic and irreversible reaction that occurs during the heating of titania [1–3]. Thus, it has been generally assumed that rutile is the thermodynamically stable phase of this compound at any temperature at 0.1 MPa [4], although Liu *et al*. have considered in a recent paper [5] that it is not certain which one is the thermodynamically stable TiO_2 polymorph at ambient conditions. To stabilize anatase or rutile in nanosized titania is a matter of great interest since for most applications, a specific particle size, morphology or crystalline structure is required [6]. Thus, nanosized rutile with a particle size around 200 nm is desired for use as a light scattering white pigment [7] because it shows a refractive index higher than anatase. However, this latter phase is the most effective as a support for a vanadia catalyst for selective o-xylene oxidation to phthalic anhydride [8–10]. Moreover, it has been found [11] that a 70 : 30 anatase : rutile mixture is the best photocatalyst for oxidation of organics in wastewater.

The above considerations explain why much work [12–17] has been concerned with the effect of different additives that would act as promoters or inhibitors of anatase → rutile conversion, provided that this reaction is very strongly dependent on impurities. The polymorphic transformation of TiO_2 induced by ball-milling at room temperature has also been reported in the literature [18–22]. Study of the evolution of the lattice defects of the two phases of titania as a function of grinding would contribute to a better understanding of the mechanism of mechanochemical conversion. The new technique of emanation thermal analysis (ETA) would be a powerful tool for this purpose [23].

ETA is based on the measurement of radon atoms released from solids previously doped with traces of ^{228}Th and ^{224}Ra. This method makes it possible to obtain information about changes in surface area, microporosity, morphology and formation of new phases taking place during sample heating or cooling. Fine and hyperfine changes in the solids and their surfaces result in changes of radon diffusivity that can be revealed under *in situ* thermal treatment conditions [23].

Description of the theory and potential of ETA has been presented elsewhere [24, 25]. The mechanisms considered for radon release from powder samples are: (i) release due to the recoil energy of the radon atoms, (ii) diffusion in open pores and in intergranular space, and (iii) radon diffusion in the matrix of the solids. The radon release rate, E (called also emanating rate), measured is therefore considered as composed of three constituents, corresponding to the release mechanism mentioned

$$E = E(\text{recoil}) + E(\text{pores}) + E(\text{matrix}) \quad (1)$$

The term E(recoil) of the emanating rate attributable to recoil can be expressed as

$$E(\text{recoil}) = K_1 \times S_1 \quad (2)$$

where K_1 is a temperature independent constant, that depends on the path of the recoiled radon atoms in the

solids and S_1 is the external geometrical surface area of the particles. The path of recoiled atoms for Rn in titania is 32 nm, the recoil energy of radon being 85 keV [26, 27].

The term $E(\text{pores})$ of the emanating rate which is due to Rn diffusion in the intergranular space and open pores can be expressed as

$$E(\text{pores}) = K_2 \times S_2 \tag{3}$$

where K_2 is a constant that depends on temperature and S_2 is the internal surface area of the sample depending on the surface of the open pores and intergranular voids.

The term $E(\text{matrix})$ of the emanating rate due to Rn diffusion in the solid matrix of the sample can be expressed as

$$E(\text{matrix}) = K_3 \exp(-Q/2RT) \times S_3 \tag{4}$$

where K_3 is a constant reflecting the atomic properties of the lattice, Q is the activation energy of Rn diffusion in the solid matrix, S_3 is the surface area representing the sum of the cross-section of all diffusion paths with the surface (dislocations, grain boundaries, etc.), R is the gas constant, and T the temperature.

The use of ETA in the characterization of the influence of grinding on textural and structural properties of titania powders constitutes the aim of the present work.

2. Experimental procedure

2.1. Materials

A sample of TiO_2 P-25 supplied by Degussa and prepared by hydrolysis of $TiCl_4$ was used [20].

2.2. Methods

A planetary ball-mill, Colerecord 20 A, with a speed of 450 r.p.m. was used. The mill was equipped with a Corindon jar (capacity 300 cm^3) containing ten balls of the same material, 20 mm in diameter. About 5 g of sample were ground in air for 5–180 min. The temperature of the jar was monitored during the grinding and it was never higher than room temperature.

On the other hand, it has been reported [20] that grinding of pure rutile under the above conditions leads to a decrease of particle size, while it is increased by heating the sample. This suggests that local heating effects do not produce the textural changes induced during the grinding of the sample. Moreover, the calcite → aragonite conversion observed in a previous paper [28], using the same ball-mill as used here, could not be explained by assuming local heating effects.

The powder X-ray diffraction spectra (XRD) of the samples were obtained with a Philips PW 1060 instrument equipped with a scintillation counter, CuK_α radiation and a nickel filter. The fraction of anatase was calculated from the following expression

$$X_A = \frac{1}{1 + 2.18(I_R/I_A)} \pm 2\% \tag{5}$$

where X_A is the fraction of anatase, and I_R and I_A are the integrated intensities of the reflections for the ⟨1 1 0⟩ plane of rutile and the ⟨1 0 1⟩ plane of anatase, respectively. This expression was determined by plotting the values of I_R/I_A, calculated from the X-ray patterns of a series of binary mixtures of both anatase and rutile as a function of X_R/X_A. Equation 5 was checked by using litharge, which has its strongest reflection at $2\theta = 28.6^\circ$, close to that of anatase, as an internal standard [29].

Both the crystalline size and the degree of microstrain of anatase and rutile have been derived from the analysis of the profile of a single diffraction line (⟨1 1 0⟩ for rutile and ⟨1 0 1⟩ for anatase) by means of the variance method [30]

$$W_{2\theta} = \frac{\lambda \Delta 2\theta}{\pi^2 D^2 \cos\langle 2\theta\rangle} - \frac{\lambda^2}{4\pi^2 D^2 \cos^2\langle\theta\rangle} + 4\langle e^2\rangle tg^2\langle\theta\rangle \tag{6}$$

where λ is the wavelength of the X-ray beam, $\langle\theta\rangle$ and $\langle 2\theta\rangle$ are the values of θ and 2θ at the centroid position, D is the crystallite size, $\langle e^2\rangle^{1/2}$ is the root-mean square strain, $\Delta 2\theta$ represents the range of the 2θ value from the X-ray profile to the centroid and $W_{2\theta}$ is the variance defined by the following expression

$$W_{2\theta} = \frac{\int_{-2\theta}^{2\theta} (2\theta - \langle 2\theta\rangle)^2 I_{2\theta}\, \mathrm{d}(2\theta)}{\int_{-2\theta}^{2\theta} I(2\theta)\, \mathrm{d}(2\theta)} \tag{7}$$

where $I(2\theta)$ is the intensity of the line profile at a given position 2θ.

The plot of $W_{2\theta}$ against $\Delta 2\theta$ would give a straight line, the slope of which gives the crystallite size and the intercept of which gives the root-mean square strain, once D is known. The computer program developed by Edwards and Toman [31] has been used.

The specific surface area was determined by the Brunaver–Emmett–Teller (BET) method using a Micromeritics surface area analyser, model 2200.

The adsorption isotherm of nitrogen, at liquid nitrogen temperature (193 K), has been measured for both the as-received and ground samples of TiO_2 after being previously outgassed at 500 °C under high vacuum (0.1 mPa). The method of the "f curves" [32] has been used for comparing the shapes of the adsorption isotherms of the ground samples with the corresponding one of the as-received sample taken as a reference material. This procedure implies that one plots the f parameter as a function of the relative adsorption pressure, P/P_0, where P represents the equilibrium pressure at which the adsorbed volume of nitrogen is V and P_0 is the saturation pressure (98 kPa for the adsorption of nitrogen at liquid nitrogen temperature). The f parameter is defined as the ratio between the volume, V, of nitrogen adsorbed on a particular sample with regards to the volume of gas, V_0, adsorbed on the reference sample at equal relative pressure. A horizontal f plot would indicate that the porous distribution of the analysed sample is similar to the corresponding one to the standard material and, therefore, the pore volume in both samples would be proportional to their corresponding specific surface areas. The deviation of the f

plot from a horizontal line would point out the change of the shape of the adsorption isotherm with regards to the reference material [32].

A Cahn electrobalance, model RG, connected to both a conventional vacuum system and a storage gas cylinder was used. A Mark II derivatograph was used as well. This system allows simultaneous recording of thermogravimetric (TG) and differential thermogravimetric (DTG) curves at pressures ranging from 0.01 to 27 kPa. The DTG results obtained in this work were recorded at a heating rate of 10 K min^{-1} and a pressure of helium gas of 20 kPa. Mass spectrometry was used to check that water vapour was the only gas product released during the heating of titania.

ETA is based on the measurement of radon atoms released from powder samples previously doped with traces of ^{228}Th and ^{224}Ra. The ETA curves were recorded by heating the labelled sample, under flow of argon gas, at a linear heating rate up to the maximum temperature selected followed by subsequent cooling to ambient temperature. The argon carrier gas swept the inert gas released by the sample into a scintillation counter and the radioactivity emanation rate measured was plotted as a function of temperature. The ETA diagrams were recorded under an argon flow of 40 cm^3 min^{-1} using a sample amount of 0.1 g. The heating and cooling rates were 5 and 2.5 K min^{-1}, respectively.

The loose powder TiO_2 samples were labelled for ETA measurements by adsorption of traces of ^{228}Th and ^{224}Ra in acetone solution (specific radioactivity of the solution 10. 000 Bq ml^{-1}) and dried at room temperature under open atmosphere. The samples were stored for three weeks prior to ETA measurement to allow radioactive equilibrium to be reached. The atoms of radon are formed as a result of the spontaneous radioactive decay according to the reaction

$$^{228}Th \xrightarrow[t_{1/2}=1.9\text{ years}]{\alpha} {}^{224}Ra \xrightarrow[t_{1/2}=3.8\text{ days}]{\alpha} {}^{220}Rn \xrightarrow[t_{1/2}=55.8\text{ s}]{\alpha} \quad (8)$$

The atoms of Rn are introduced into the TiO_2 powder sample to a maximum depth of 32 nm due to the recoil energy of 85 keV that every atom gains during its formation by the nuclear reaction of alpha radioactive decay [26, 27]. The double recoil effect is used here for the introduction of radon into the surface layers of the sample, namely the recoil of ^{224}Ra and ^{220}Rn, respectively.

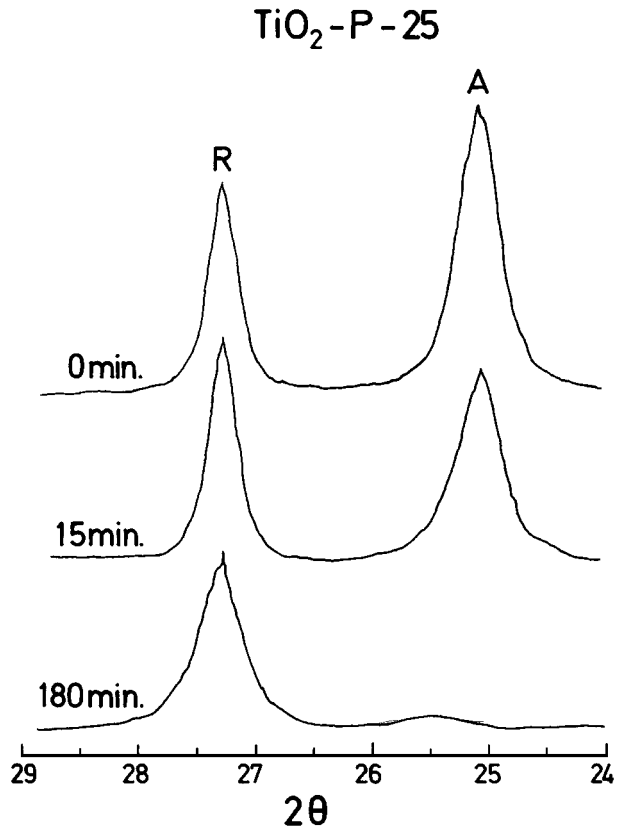

Figure 1 X-ray diffraction patterns of the as-received and ground samples of TiO_2: (A) anatase, (R) rutile.

3. Results and discussion

The surface areas calculated for both the as-received and ground samples of TiO_2 are included in Table I together with their corresponding percentages of anatase/rutile, crystallite sizes and microstrain levels as determined from the XRD diagrams represented in Fig. 1. The average particle diameter calculated from the surface area data, taking into account the theoretical density of anatase and rutile and assuming spherical symmetry, are also included in Table I. These results suggest that an increase of particle size as a function of grinding takes place. This is roughly in agreement with the TEM pictures shown in Fig. 2. These results could

TABLE I Characteristics of the three samples of TiO_2

Grinding time (min)	Anatase (%)	S_{BET} (m^2 g^{-1})[a]	D_{BET} (nm)[b]	D (nm)[c]		$\langle e\rangle \times 10^{-3}$ [d]		Weight loss up 500 °C (%)
				Anatase	Rutile	Anatase	Rutile	
0	48	53.7	27.4	104	125	3.6	2.6	1.4
15	38	52.6	27.2	85	140	4.5	2.4	1.4
180	0	34.1	41.4	—	80	—	4.5	0.9

[a] S_{BET}, surface area.

[b] D_{BET}, particle size determined from S_{BET}. The particle diameter has been determined from the expression: $D_{BET} = (6/\rho S_{BET}) \times 10^4$ nm, ρ being the density of the material calculated from the theoretical density of anatase (3.893 g cm^{-3}) and rutile (4.250 g cm^{-3}) after taking into account the composition of the sample.

[c] D, crystallite size.

[d] $\langle e\rangle \times 10^{-3}$, microstrain calculated from the XRD diagrams using the Varianze method.

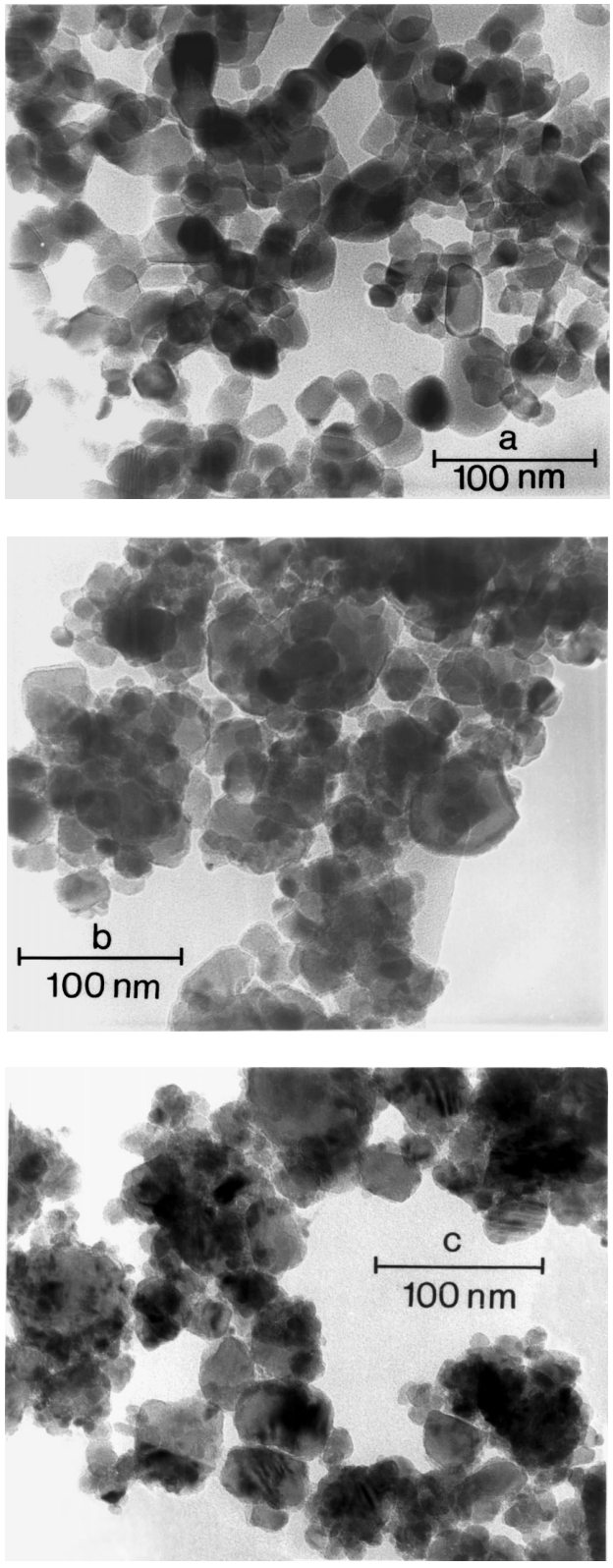

Figure 2 TEM pictures of the as-received and ground samples of TiO_2: (a) 0 min, (b) 15 min, and (c) 180 min.

be interpreted by assuming that the lattice defects generated during the grinding process promote cold-welding of the particles. Moreover, Table I points out that a decrease of the crystallite size of anatase takes place during the grinding process at the time that their corresponding microstrain level increases. This behaviour can be understood by assuming that the particles of the powder samples are formed by small crystallites welded in a mosaic structure and that the grain boundaries constitute the main contribution to the microstrains. The fact that the particle sizes determined from surface area measurements are considerably higher than the corresponding crystallite sizes calculated from XRD broadening seems to support this statement. This interpretation is similar to those given in previous papers in which an inverse relationship between the crystallite size and the microstrain level of a number of materials has been reported [29, 33, 34]. The increase of crystallite size of rutile (with its associated decrease of microstrain level) after 15 min of grinding can be explained by assuming that the anatase anneals the excess energy stored by the lattice imperfections generated during mechanical treatment by undergoing a polymorphic transformation into a better crystallized rutile. These results are in very good agreement with those reported in previous papers [35, 36], which conclude that the rutile particles obtained by phase transition are always much larger than both the starting and the residual anatase particles. A monotonous decrease of the rutile crystal size would be expected if grinding continues in progress. This behaviour explains why the crystallite size of this phase decreases down to 80 nm after a grinding time of 180 min.

Fig. 3 shows the f plots that have been obtained from nitrogen adsorption isotherms of the ground TiO_2 samples after taking the as-received sample as a standard. The fact that they are straight horizontal lines suggests that the volume distribution of pores does not change during the grinding process; this is supported by the fact that the specific surface area changes taking place during the grinding of titania are motivated by particle size modifications.

If we consider the large specific surface of the titania samples studied here, it would be expected that they take up a significant amount of water vapour from the open atmosphere. Taking into account that this phenomenon can influence the rate of radon emanation during the recording of ETA experiments it would be interesting to follow the water desorbed by both the

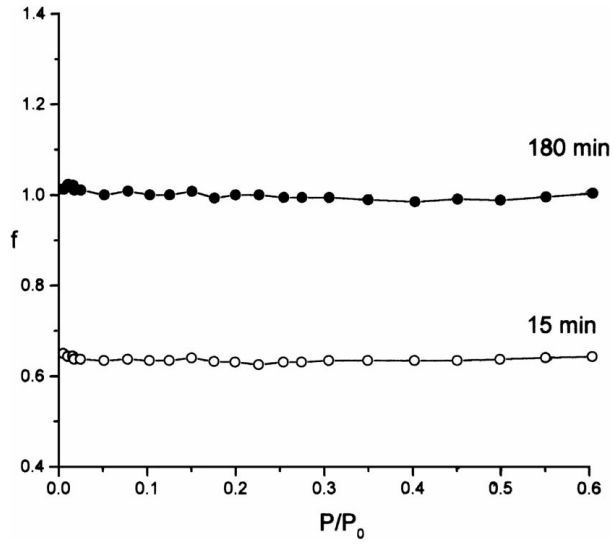

Figure 3 f plots of ground TiO_2 samples obtained using as standard the as-received sample of TiO_2.

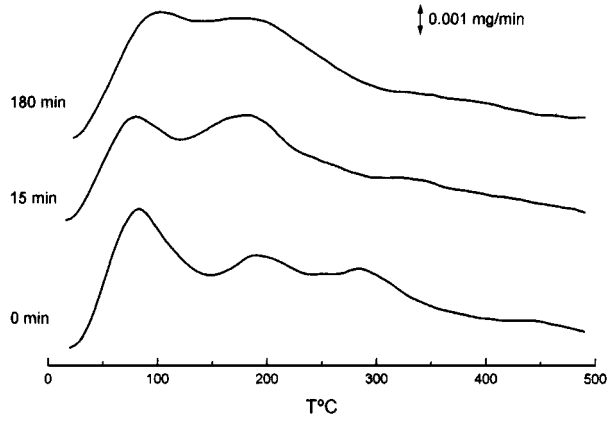

Figure 4 DTG curves showing the desorption of water from the TiO_2 sample as a function of grinding time.

as-received and ground samples of titania as a function of temperature. The values of the total weight loss up to 500 °C, as calculated from the TG diagrams of these samples are shown in Table I. The resolution power of DTG for discriminating overlapping processes is considerably higher than the corresponding one of TG. Thus, the DTG curves of both the as-received and ground TiO_2 samples have been chosen for representation in Fig. 4.

The XRD patterns of the as-received TiO_2 sample were obtained at room temperature after 1 h of heating at increasing temperatures. Fig. 5 shows the plots of both the fraction of anatase, as calculated from Equation 1, and the specific surface as a function of temperature.

The ETA results are presented as the temperature dependence of the radon release rate, E, normalized to the total radioactivity of the parent nuclides adsorbed on the sample surface by labelling. Fig. 6 shows the ETA diagrams recorded at temperatures ranging from 20 to 1100 °C under heating and cooling conditions.

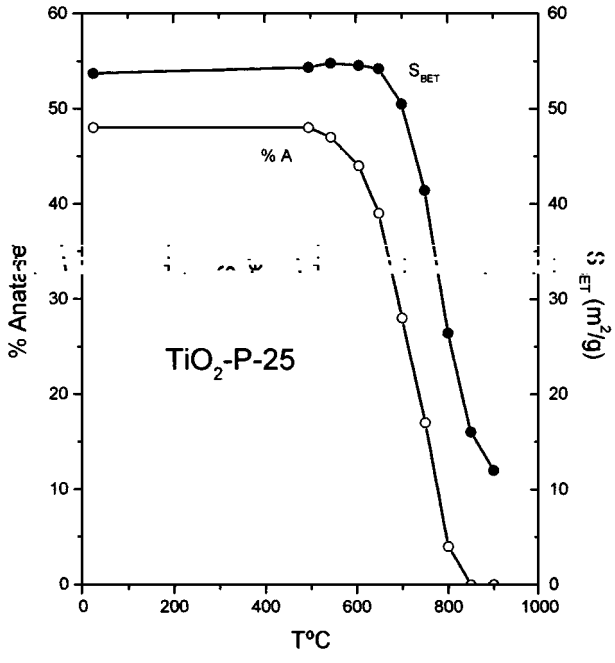

Figure 5 Weight fraction of anatase and specific surface area of the as-received TiO_2 after heating for 1 h at different temperatures.

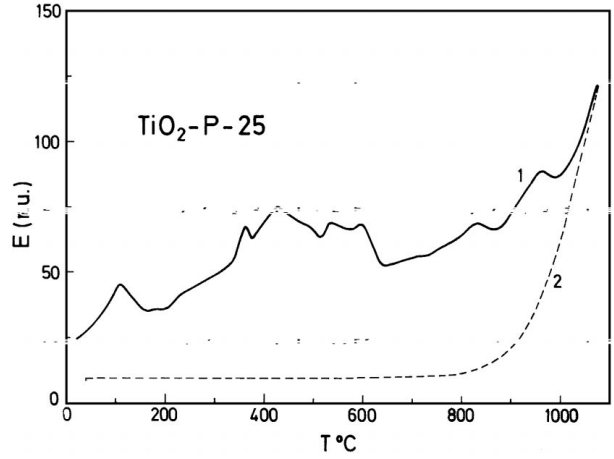

Figure 6 ETA curves of TiO_2 sample, as-received, measured during heating from 20 to 1100 °C and subsequent cooling in air: (1) heating at a rate of 5 K min^{-1}, (2) cooling at a rate of 2.5 K min^{-1}.

It is well known that bulk ionic diffusion does not start until the Tamman temperature, which is very close to half of the melting point of the solid [37]. Thus, the radon release rate on TiO_2 at temperatures lower than 700 °C should be ascribed to recoil and diffusion in the intergranular space and open pores as described by Equations 2 and 3, respectively. Thus, the ETA curves at this temperature range mainly reflect the changes undergone by the surface properties of the sample. At temperatures higher than the Tamman temperature, radon release due to its diffusion in the bulk, as given by the exponential law expressed by Equation 4, represents the main contribution to the absolute value of E. Therefore, the transport properties of the material overlap with the textural properties in this temperature range of the ETA curve.

The E value measured at room temperature, E_{25}, depends on the surface area, the roughness of the titania grains and the morphology of the agglomerated grains. The presence of adsorbed water on the sample surface results usually in a decrease of the E_{25} value [38]. This is due to the fact that part of the radon atoms released from the solid grains and their surfaces by recoil is stopped in the water layer adsorbed on the sample.

In the temperature interval 20–100 °C a release of adsorbed water takes place, as indicated by the corresponding DTG curve in Fig. 4. This is reflected by an increase in the radon release rate in the respective temperature interval on the ETA curve of Fig. 6. In addition it should be mentioned that the water adsorbed in pores and intergranular spaces contains a rather high concentration of ^{224}Ra, being the parent nuclide for ^{220}Rn. Thus, the water removed during heating of the sample up to 110 °C leads to an additional increase of the radon release rate; accordingly, a diminution of E is observed when the water desorption rate decreases again. The DTG peaks corresponding to desorption of water recorded at this range of temperatures roughly agree with this interpretation.

The increase of E in the temperature interval 200–350 °C is controlled by the thermal diffusion of radon in open pores and intergranular interstices overlapping with the emanation rate, originated by desorption of

the strongest form of adsorbed water taking place in this temperature range, as Fig. 4 shows. The enhancement of E from 350 to 380 °C, followed by a decrease of this parameter up to 500 °C, is associated neither with water release nor with the decrease of specific area as shown by Figs 4 and 5. These effects can be ascribed to the reordering or annealing of surface defects of titanium dioxide and to changes in the morphology of the grain agglomerates that are not associated with a change of the total external area. This assumed behaviour is similar to the one reported from high resolution HRTEM analysis of ribbons of Fe–Cr–Ni austenitic alloys annealed at temperatures lower than the Tamman temperature [39]. At higher temperatures the annealing of emergent dislocations with consequent recrystallization of the material was observed [39]. The small particle sizes of the TiO_2 powders here studied makes it very difficult to perform HRTEM observations.

The diminution of the radon release rate at temperatures ranging from 500 to 700 °C can be ascribed to rearrangement of lattice defects in the bulk oxide prior to the ETA effects observed at temperatures ranging from 750 to 850 °C. This last effect is caused by anatase → rutile polymorphic transformation (taking place at this temperature, as checked by XRD) and by the dramatic decrease of the specific surface, as Fig. 5 shows. The fact that the change of textural and structural properties shown in Fig. 5 takes place at slightly lower temperatures than that assumed for these phenomena in Fig. 6 can be easily explained taking into account the different heating schedule used for recording both sets of data. Thus, the results of Fig. 4 were obtained after 1 h of cumulative and consecutive isothermal heating at increasing temperatures, while the ETA diagram of Fig. 6 was obtained under a linear heating rate of 10 °C min^{-1}. It is well known [40] that the temperatures at which an activated process occurs move to higher values by increasing the heating rate. Finally, the increase of E in the temperature interval 970–1070 °C reflects the further densification of the material by annealing of pores isolated in intergranular cavities formed between particles welded during the sintering process. The fact that this thermal effect is also observed (in the ETA diagram included in Fig. 9, to be discussed later) for the TiO_2 sample ground for 180 min, which is constituted of pure rutile, supports the previous assumption, provided that this sample cannot undergo a phase change.

The ETA curve of Fig. 6 shows that all the textural and structural changes reported are not reversible. On the other hand, it has been previously shown (see Equation 4) that the bulk diffusion of radon is characterized by an exponential relationship between the radon emanation rate and $1/T$, leading to an activation energy that depends on the concentration of reticular defects and the densification of the material. Thus, the analysis of the ETA cooling curves, recorded after previous annealing of the TiO_2 sample at different temperatures, could perhaps be used to follow the concentration trend of lattice imperfections, provided that the other processes that overlap them have been removed during the previous heat treatment.

Fig. 7 shows the ETA traces obtained during heating of the as-received TiO_2 sample up to 400 °C and subsequent cooling to room temperature. The heating and cooling ETA diagrams recorded in the temperature interval 20–1000 °C for the same sample preheated at 700 °C for 1 h are also included in Fig. 7. These results point out that prior heating of the sample at a particular temperature anneals the effects recorded on the ETA curve up to this temperature, but does not anneal the textural and structural modifications occurring at higher temperatures. Thus, the irreversibility of the different ETA effects shown in Fig. 6 is confirmed.

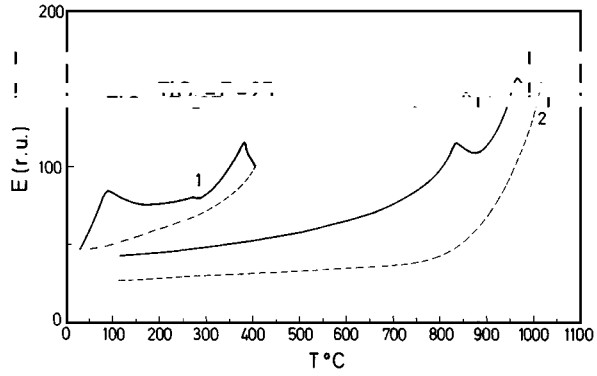

Figure 7 ETA curves of the as-received TiO_2 sample at subsequent thermal treatments in air at the following temperatures intervals: (1) heating from 20 to 400 °C with subsequent cooling in air, (2) heating from 20 to 1000 °C with subsequent cooling in air of the sample preheated to 700 °C.

The temperature dependence of the radon release rate values taken from cooling curves 1 and 2 of Fig. 7 are represented in Fig. 8 as a semilogarithmic plot, i.e. $\log(E - E_{25})$ versus $1/T$. It can be observed that the radon activity of the sample preheated at 1000 °C is considerably lower than the corresponding activity of the sample preheated at 400 °C. This behaviour could be explained by considering that the higher the sample is heated, the lower the concentration of lattice imperfections will be. On the other hand, Fig. 8 shows that an abrupt exponential increase of the radon emanation rate is observed in the 300–400 °C region of the curve recorded during cooling from 400 °C of the TiO_2 compound previously annealed at this temperature. This behaviour can only be explained by assuming that the emanating rate is due to radon diffusion

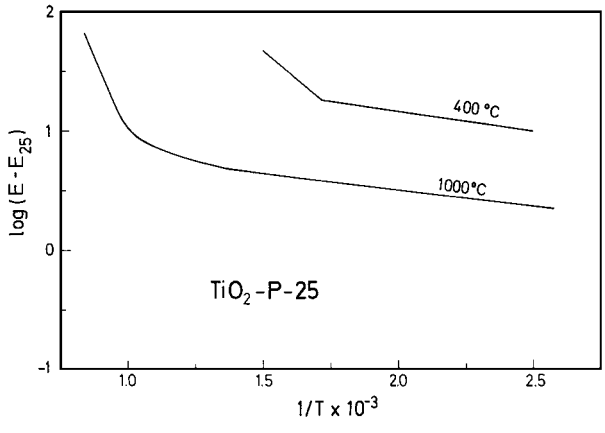

Figure 8 Temperature dependence of $\log(E - E_{25})$ versus $1/T$ plotted from the values of E measured during cooling of the as-received sample after thermal treatment at 400 °C and 1000 °C.

in the solid bulk according to Equation [4]. A value of $Q = 43.0$ KJ mol^{-1} has been determined from curve 1 in Fig. 8 radon diffusion for the activation energy. It is noteworthy that the exponential decay of the radon emanation rate on the cooling curve of the sample preheated at 1000 °C (curve 2, Fig. 8) continues to progress from this temperature down to 770 °C, leading to an activation energy $Q = 254.1$ KJ mol^{-1} for the diffusion of radon through the titania matrix. The difference between these two Q values clearly demonstrates the change in the concentration of lattice defects as a consequence of heat treatment.

The ETA profiles of the ground TiO_2 samples up to 700 °C present similar characteristics to those shown in Fig. 7 by the as-received one. We must bear in mind that the bulk diffusion of radon, which is dependent on the lattice defect concentration, starts at temperatures around 700–800 °C. Thus, it is of special interest to compare the ETA curves at temperatures ranging from 700 to 1100 °C in order to analyse the influence of grinding on the texture and structure of TiO_2. Fig. 9 shows the heating ETA curves recorded in the temperature interval 700–1100 °C for samples ground for 15 and 180 min, together with their subsequent cooling curves from 1000 °C down to room temperature. It can be observed that the ETA effects that appear at about 800 °C on the heating curve of the as-received sample do not appear on the corresponding curves recorded for the ground samples. This effect was ascribed to the anatase → rutile transformation, and cannot be observed in the ETA diagram of the TiO_2 ground for 180 min, because the anatase was completely transformed into rutile during the grinding treatment. On the other hand, the data included in Fig. 10 show that

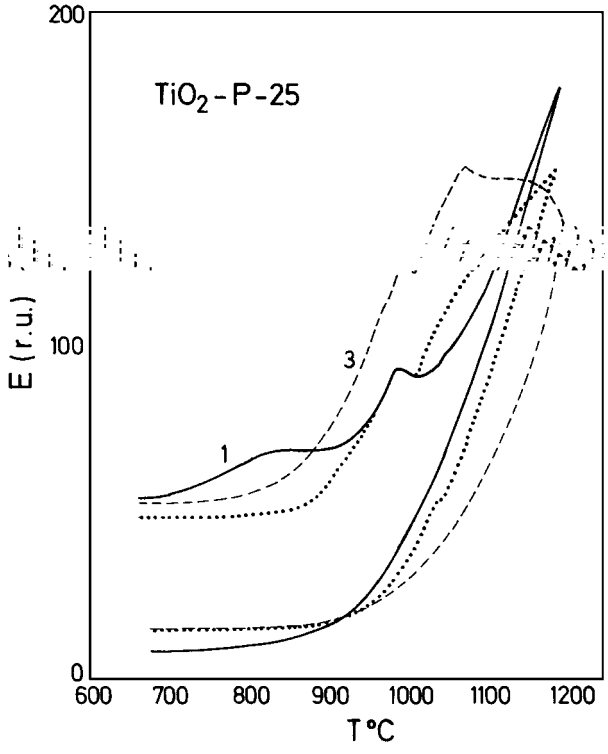

Figure 9 ETA curves of TiO_2 samples measured during heating from 700 to 1100 °C and subsequent cooling in air: (1) as-received, (2) ground for 15 min, and (3) ground for 180 min.

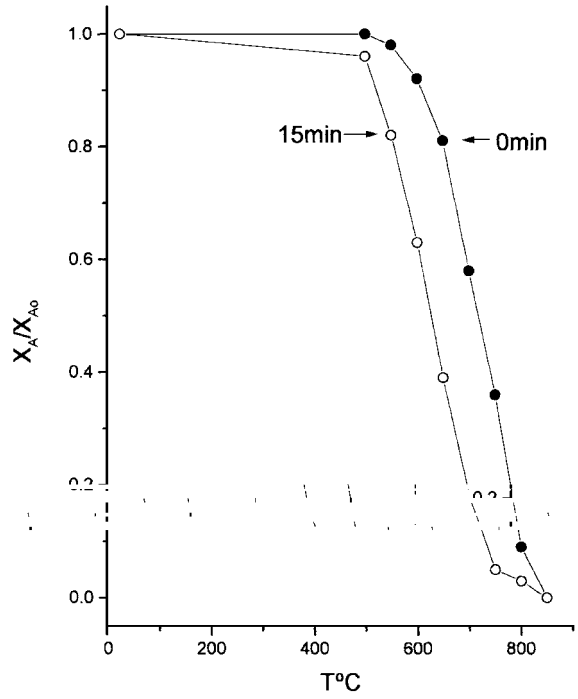

Figure 10 Weight fraction of anatase, initially contained in the as-received and ground samples of TiO_2, which has been converted to rutile after heating for 1 h at different temperatures.

the anatase remaining in the sample ground for 15 min transforms into rutile at lower temperatures compared with the ungrounded sample. This behaviour could be easily understood taking into account the lower crystallite size of anatase in the ground sample with regards to the as-received one [35]. A comparison of the heating curves included in Fig. 9 points out that the radon emanation rate increases with increasing grinding time. This is true in spite of the fact that the radon emanation rate attributable to recoil and diffusion through intergranular spaces and open pores is proportional to the specific surface area, which decreases during the mechanical treatment as shown in Table I. Therefore, the augmentation of E must be mainly ascribed to the increasing concentration of lattice defects created during the grinding process at room temperature, according to the results reported in Table I. It is necessary to remark that comparison of the ETA cooling curves of Fig. 9 indicates that the radon emanation rate of the samples previously annealed at 1100 °C decreases with increasing grinding time. Table II shows the activation energy of the bulk diffusion of radon calculated from the exponential part of the plot of the log $(E - E_{25})$ values taken from the cooling curves of Fig. 9 as a function of the corresponding $1/T$ values. These results confirm that the activation energy for the bulk diffusion of radon into the TiO_2 samples annealed at 1100 °C increases with

TABLE II Activation energy of the bulk diffusion of radon calculated from the cooling curves of as-received and ground samples of TiO_2 shown in Fig. 8

Sample of TiO_2	E (KJ mol^{-1})
As-received	254
Ground for 15 min	283
Ground for 180 min	320

increasing prior grinding time at room temperature. This behaviour can be interpreted by considering that the temperature at which the crystals start to grow decreases with the increasing initial concentration of lattice defects in the material as a function of grinding time.

In summary, although the starting degree of crystallinity of the as-received TiO_2 sample is initially higher than the degree of crystallinity in the ground samples, annealing out of crystal defects during heating treatment at 1100 °C makes the previously milled powders more perfect materials than the as-received one. A similar behaviour has been previously reported for the annealing of a series of nickel samples with different concentrations of microstrains, as measured from XRD experiments [33]. It was demonstrated that the higher the concentration of defects is, the lower the temperature at which broadening of the XRD profiles starts to decrease. This interpretation is also supported by the results reported in [2, 35, 41], which show that the smaller the crystallite size of anatase, the lower is the temperature at which both crystal growth and phase transformation into rutile starts.

4. Conclusions

The results indicate that ETA is a suitable method for characterization of the processes that take place during thermal treatment of ceramic materials like TiO_2. Moreover, the results suggest that determination of activation energy for the diffusion of radon in a titania matrix could provide valuable information about crystal imperfections. On the other hand, a comparison of radon diffusion release, obtained as a function of temperature from a series of labelled TiO_2 samples submitted to different mechanical treatments, allows us to conclude that the ETA method is very sensitive to the concentration of lattice imperfections. Therefore, this technique could be used for comparing the relative concentration of lattice defects in the bulk of a series of materials after being submitted to different thermal or mechanical treatments.

References

1. A. W. CZANDERNA, C. N. R. RAO and J. M. HONJG, *Trans. Faraday Soc.* **54** (1958) 1069.
2. K. N. P. KUMAR, K. KEIZER, A. J. BARGGRAAF, H. NAGAMOTO and S. MOROOKA, *Nature* **358** (1992) 48.
3. I. BARIN, in "Thermochemical Data of Pure Substances" (Verlag Chemie, Berlin, 1995).
4. R. D. SHANNON and J. A. PASKS, *J. Amer. Ceram. Soc.* **48** (1965) 395.
5. L. G. LIU and T. P. MERRAGH, *Eur. J. Mineral.* **4** (1992) 45.
6. A. J. RILISON, P. F. NIQUEL and J. L. KATZ, *J. Mater. Res.* **11** (1996) 3083.
7. J. H. BRAUN, A. BAIDINS and B. E. MARGANSKI, *Prog. Org. Coat.* **20** (1992) 1051.
8. M. S. WAINWRIGHT and C. R. FOSTER, *Catal. Rev.* **19** (1979) 211.
9. G. C. BOND and S. TAHIR, *Appl. Catal.* **71** (1991) 1.
10. G. DEO, A. M. TAREK, I. E. WACHS, T. MACKEJ, J. HABER, N. DAS, H. ECKEST and A. M. HIRT, *Appl. Catal. A* **91** (1992) 27.
11. R. J. BERRJ and M. R. MUELLER, *Microchem. J.* **50** (1994) 28.
12. G. BESCA, G. RAMIS, J. M. GALLARDO, V. S. ESCRIBANO and P. PIAGGIO, *J. Chem. Soc., Faraday Trans. I.* **90** (1994) 3181.
13. F. GARBASSI, E. MELLO CERESA, E. OCCHIET, L. POZZI, M. VISCA and D. M. LENTI, *Langmuir* **3** (1987) 173.
14. A. K. VASUDEVAN, P. P. RAO, S. K. GHOSH, G. M. ARILKUMAR, A. D. DAMODARAN and K. G. K. WARRIER, *J. Mater. Sci. Lett.* **16** (1997) 8.
15. A. M. VENEZIA, L. PALMISANO and M. SCHIAVELLO, *J. Solid State Chem.* **114** (1995) 364.
16. R. DEBNATH and J. CHANDHURI, *J. Mater. Res.* **7** (1992) 3348.
17. J. ANDRADE-GAMBOA and D. M. PASQUENCH, *J. Amer. Ceram. Soc.* **75** (1992) 2934.
18. Y. TEKIZ and C. LEGRAND, *C. R. Acad. Sci.* **2611** (1965) 8.
19. T. KUBO, M. KATO, Y. MITARI, Y. TAKAHASHI and K. OHKURA, *J. Chem. Soc. Jpn, Ind. Chem. Soc.* **3** (1963) 66.
20. J. M. CRIADO and C. REAL, *J. Chem. Soc. Faraday Trans. I* **79** (1983) 2765.
21. J. M. CRIADO, C. REAL and J. SORIA, *Solid State Ionics* **32/33** (1989) 461.
22. S. BEGIN-COLIN, L. R. ARAUJO-PORTS, G. LECAËR, A. PIARELLI and P. MATTEAZZI, in "Proceedings of the 18th International Conference on Mechanochemistry," Vol. 2 (Cambridge Interscience, 1993) p. 51.
23. V. BALEK, E. KLOSOVA, M. MURAT and N. A. CAMARGO, *Amer. Ceram. Soc. Bull.* **75** (1996) 73.
24. V. BALEK, *Thermochim. Acta* **192** (1991) 1.
25. V. BALEK and J. TÖLGYESSI, in "Emanation Thermal Analysis and Other Radiometric Emanation Methods," in Wilson and Wilson's "Comprehensive Analitycal Chemistry, Part XII C" (Elsevier, 1984) p. 304.
26. *Idem, ibid.* p. 49.
27. N. BOHR, K. G. L. DANSKE VIDENSKAL, *Selkal Mat. Fyz. Medd.* **18** (1948) N8.
28. J. M. CRIADO and J. M. TRILLO, *J. Chem. Soc. Faraday Trans. I* **71** (1975) 961.
29. J. M. CRIADO, M. GONZALEZ and C. REAL, *J. Mater. Sci. Lett.* **5** (1986) 467.
30. H. P. KLUG and L. E. ALEXANDER, in "X-ray Diffraction Procedures for Polycrystalline and Amorphous Materials" (Wiley, New York, 1974) p. 660.
31. H. E. EDWARDS and K. TOMAN, *J. Appl. Cryst.* **2** (1969) 240.
32. S. I. GREEG, *J. Chem. Soc. Chem. Comm.* (1975) 699.
33. J. M. CRIADO and M. J. DIANEZ, *J. Mater. Sci.* **2** (1991) 821.
34. M. J. DIANEZ, J. CARRION and J. M. CRIADO, in "Proceeding of the First International Conference on Mechanochemistry" (Cambridge Interscience, 1993) p. 153.
35. J. M. GALLARDO-AMORES, V. SANCHEZ-ESCRIBANO and G. BUSCA, *J. Mater. Chem.* **5** (1995) 1245.
36. L. E. DEPERO, P. BONZI, M. ZOCCHI, C. CAZALE and G. DE MICHELE, *J. Mater. Res.* **8** (1993) 2709.
37. N. N. GREENWOOD, in "Ionics Crystals Lattice Defects and Non-Stoichiometry" (Butterworth, London, 1968) p. 165.
38. V. BALEK and J. TOLGYESY, in "Emanation Thermal Analysis and other Radiometric Emanation Methods," in Wilson and Wilson's "Comprehensive Analitycal Chemistry, Part XII C" (Elsevier, 1984) p. 59.
39. J. M. CRIADO, E. J. HERRERA and J. M. TRILLO, in "Catalysis," edited by J. W. Highfower (Elsevier, New York, 1973) pp. 541–555.
40. M. E. BROWN, "Introduction to Thermal Analysis: Techniques and Applications" (Chapman & Hall, New York, 1988) pp. 144–50.
41. X. Z. DING, X. H. LIN and Y. Z. HE, *J. Mater. Sci. Lett.* **15** (1996) 1789.

Received 15 July 1997
and accepted 30 July 1998